Title: Intrastriatal delivery of a zinc finger protein targeting the mutant HTT gene obviates lipid phenotypes in zQ175DN HD mice

Authors: Andrew Iwanowicz*[1], Adel Boudi*[1], Connor Seeley*[1], Ellen Sapp*, Rachael Miller[Ŧ], Sophia Liu*, Kathy Chase [Ŧ], Kai Shing*, Ana Rita Batista[&], Miguel Siena-Esteves[&], Neil Aronin[Ŧ], Marian DiFiglia*, Kimberly B. Kegel-Gleason*[|]

*Department of Neurology, Massachusetts General Hospital, Charlestown, MA
[Ŧ] RNAi Therapeutics Institute, University of Massachusetts Medical School, Worcester, MA
[&] Department of Neurology and Horae Gene Therapy Center, University of Massachusetts Chan Medical School
[1]These authors contributed equally.

[|]**Corresponding Author:** Kimberly B. Kegel-Gleason, PhD
114 16th Street, Room 2001
Charlestown, MA 02129
Tel: 617-724-8754
Email: kkegelgleason@mgh.harvard.edu

Abstract: Reducing the burden of mutant Huntingtin (mHTT) protein in brain cells is a strategy for treating Huntington's disease (HD). However, it is still unclear what pathological changes can be reproducibly reversed by mHTT lowering. We previously found that lipid changes that occur with HD progression could be prevented by attenuating HTT transcription of the mutant allele in a genetic mouse model (LacQ140) with inducible whole body lowering. Here, we tested whether intrastriatal injection of a therapeutic capable of repressing the mutant *HTT* allele with expanded CAG can provide similar protection against lipid changes in HD mice with a deletion of neo cassette (zQ175DN).

Methods: Wild-type or zQ175DN mice were injected with AAV9 bearing a cDNA for a zinc finger protein (ZFP) which preferentially targets mutant HTT (ZFP-HTT) to repress transcription (Zeitler et al., 2019). Proteins were analyzed using western blot, capillary electrophoresis, and nitrocellulose filtration methods. Lipid analyses were conducted by liquid chromatography and mass spectrometry (LC-MS). Somatic expansion index was assessed using capillary gel electrophoresis of PCR products.

Conclusions: Lowering mHTT levels by 43% for 4 months prevented numerous changes in lipids of caudate-putamen in zQ175DN mice. Our data support the idea that mHTT lowering can provide meaningful benefits and support brain health. Furthermore, our data demonstrate that analyzing lipid signatures is a valuable method for evaluating potential therapies in a preclinical model of HD.

Key words: AAV9, striatum, Huntington's disease, transcription, metabolomics, gene therapy

Funding: CHDI Foundation, Dake Family Fund

Acknowledgements: We thank David Howland and Deanna Marchionini at CHDI Foundation for helpful advice and Jonathon Asara at the Beth Israel Deaconess Medical Center Mass Spectrometry Core for help with LC-MS and lipid annotation.

Introduction

A heritable mutation causing abnormal expansion of a normal CAG repeat sequence in the *HTT* gene causes Huntington's disease (HD) (1993), a neurodegenerative disease in which patients suffer progressive cognitive, psychiatric, and motor symptoms, and ultimately death (Ross and Tabrizi, 2011). Further CAG repeat expansion can happen in individual cells with age (somatic instability, SI), and genes involved in DNA mismatch repair were identified as modifiers of age of onset in human Genome Wide Association Studies(GWAS) (Genetic Modifiers of Huntington's Disease Consortium, 2019;Lee et al., 2022).

Neurodegeneration has been attributed to numerous mechanisms. The CAG expansion results in extension of a normal polyglutamine tract in the protein, Huntingtin (HTT), producing abnormal protein function and interactions, misfolding, and aggregation. The CAG expansion can also drive expression of a short "readthrough" mRNA, which fails to splice correctly and uses a cryptic stop site present within intron1 (Sathasivam et al., 2013). This small mRNA can accumulate in nuclear clusters (Fienko et al., 2022) and can be translated to a short protein product bearing expanded polyQ, which may seed aggregation thought to contribute to pathology (Landles et al., 2010). Finally, the CAG repeat itself could directly affect neuron health by affecting local chromatin architecture (Alcala-Vida et al., 2021) or through changes in epigenetic regulation (reviewed by (Hyeon et al., 2021)).

Because mutant *HTT* gene products may be involved in diverse pathological mechanisms, one approach is to block the expression of *HTT* gene products using gene therapy approaches. One path is to reduce RNA and protein by targeting the level RNA using synthetic antisense oligonucleotides (ASOs) (Carroll et al., 2011;Kordasiewicz et al., 2012;Southwell et al., 2018), microRNAs (miRs) (Keeler et al., 2016), or small interfering RNAs (siRNAs) (Alterman et al., 2019;Conroy et al., 2022). Another approach is to target the *HTT* gene directly at the level of transcription using proteins engineered to bind the mutant allele, such as a zinc finger protein (ZFP) (Zeitler et al., 2019). This approach has the advantage of blocking all gene products, including the small Htt1a readthrough product. Gene editing with CRISPR caspase systems may be curative if delivery methods to the brain can be improved.

The question of how early to treat, how much lowering is needed and how long it should sustain has remained unclear, although it is a subject of intense interest. The effects of lowering both normal and mutant HTT remains a concern due to the diverse roles of WT HTT in brain function. Preclinical studies in mice have used various methods to lower total (normal and mutant) HTT levels including ASOs and siRNAs. Lowering mHTT specifically has been more difficult but has been achieved with ZFPs in mice and siRNA and ASOs in human stem cells that contain certain single nucleotide polymorphisms (Mathkar et al., 2019;Conroy et al., 2022). The routes of delivering the lowering agent to the nervous system in mice include injection into the lateral ventricle or the caudate-putamen. These methods achieved substantial lowering of mHTT (70-99%) in some brain regions (Carroll et al., 2011;Kordasiewicz et al., 2012;Southwell et al., 2018;Zeitler et al., 2019). The readouts used to assess the effects of HD gene lowering in the aforementioned studies include mRNA levels for striatal genes known to change in HD (PDE10 and DARPP32) (Stanek et al., 2013), immunofluorescence for DARPP32, ligand binding to PDE10, dopamine receptors 1 and 2) (D1R and D2R) (Zeitler et al., 2019), brain mass, volume of caudate-putamen, the presence of inclusions formed by mHTT, and behavioral and cognitive measures all

assessed at one or two time points post treatment (Carroll et al., 2011;Kordasiewicz et al., 2012;Southwell et al., 2018).

The protective effects of mHTT lowering on various disease markers have had mixed results despite significant reductions in mHTT. Direct injection of AAV with sequence encoding a ZFP into the caudate-putamen to target HD gene transcription profoundly reduced mHTT levels by 98%, but demonstrated modest recovery of ligand binding to D1R, D2R, and PDE10a, and partial recovery of immunofluorescence for DARPP32 (Zeitler et al., 2019). ASOs introduced into transgenic HD models (BACHD, YAC128 and R6/2) provided 75-84% mHTT lowering and improved behavioral and cognitive readouts, prevented the loss of brain volume and/or mass, retention of DARPP32 levels and increased mouse viability (Carroll et al., 2011;Kordasiewicz et al., 2012;Southwell et al., 2018).There was limited improvement in reversing changes in levels of mRNA transcripts specific to striatal medium spiny neurons (MSN) (Stanek et al., 2013).

Many of the experimental readouts reported in studies using HD mouse models are semi-quantitative, have high variability requiring numerous mice and are labor intensive. RNAseq or microarray analysis are quantitative and give strong, reproducible phenotypes in HD mouse models (Luthi-Carter et al., 2000;Langfelder et al., 2016). In another study, only partial reversal of the transcriptomic signature occurred with a genetic inducible model of mHTT lowering which lowered in all cell types (LacQ140; (Marchionini et al., 2022)). Using the highly accurate and quantitative method of liquid chromatography and mass spectrometry (LC-MS), we recently demonstrated in the LacQ140 mice that significant changes in levels of numerous lipids occurred, and reducing mHTT levels was protective (Shing et al., 2023). Here, we tested whether the benefits of a potential therapeutic could be evaluated using LC-MS to track global lipid changes.

Methods and Materials

Animal Welfare Statement

All the studies in this manuscript were conducted in compliance with the Institutional Care and Use Committee (IACUC) guidelines of the University of Massachusetts Chan Medical School (docket #202100018).

AAV subcloning & packaging

The zinc finger protein (ZFP) cDNA constructs were originally created by Sangamo were engineered to bind to the HTT gene with specificity for expanded CAGs fused to the repressor domain of the KRAB protein (ZFP-HTT) (Zeitler et al., 2019)and were provided by CHDI Foundation. This fusion protein has been shown to selectively repress transcription from the mutant HTT allele containing high CAG repeats including the HTT1a exon1-intron1 readthrough transcript (Zeitler et al., 2019). The cDNA encoding construct “30645” specific to mutant HTT (ZFP-HTT) with an N-terminal FLAG tag was fused in frame with the KRAB repressor domain (Construct D from Zeitler B. Nature Med 2019) and subcloned into a self-complimentary adeno associated virus 9 (AAV9) vector, with expression driven by a CBA promoter fused to a CMV enhancer (Figure 1). The DNA binding domain (DBD) from this construct was deleted to serve as a control (ZFP-dDBD) (described by Zeitler B. Nature Med 2019) was also subcloned into the same viral vector. The resulting vectors named scAAV9-CB-ZFPHtt and scAAV9-CB-ZFPDBD were

produced and purified as previously described (Batista et al., 2020). Vector titer was determined by quantitative PCR (qPCR) using primers and probes for the polyadenylation signal.

Mouse Intracranial Injection Surgeries

Heterozygous zQ175DN HD mice (abbreviated to Q175/Q7 in figures and tables) and their wild-type (WT) littermate controls (Q7/Q7) were purchased from The Jackson Laboratories (Z_Q175 KI (neo-); (C57BL/6J)- CHDI stock # 370832, JAX stock #029928). The knock-in zQ175/Q7 mouse model was isolated as a natural variant in progeny of the Q140 knock-in mouse model and expanded (Menalled et al., 2003;Menalled et al., 2012); the model was created by homologous recombination of mouse exon1 with human exon1 containing an expanded CAG expansion in the HTT allele. The neo cassette which suppress expression of the mutant HTT allele (Southwell et al., 2016) was deleted to create zQ175/Q7 DN mice which express mHTT at endogenous levels. All animals were maintained and used according to the Institutional Animal Care and Use Committee guidelines of the University of Massachusetts Chan Medical School (docket #20210018). Briefly, mice were housed with a maximum of 5 per cage in a pathogen-free facility under standard conditions with access to food, water, and enrichment *ad libitum.* At eight weeks of age, mice were anesthetized with 284 mg/kg tribromoethanol (Avertin) and placed into a small animal stereotaxic apparatus (ASI Instruments and WPI Instruments). Microinjector pumps were fastened to the stereotaxic and set to deliver 2.5µL bilaterally (5µL total) of AAV9 virus ($3.5x10^{10}$ PFU) at a rate of 500 nL/min. Our previous studies show that this dose results in near complete coverage of the caudate-putamen in mice. The surgical position was set using the bregma as the zero position for guidance, then measured ± 2.0 mm medial-lateral and +1.0 mm anterior-posterior (AP), and finally lowered -3.0 mm dorsal-ventral (DV) into the striatum. The injections were started one minute after the needle was inserted, and the needle was removed one minute after the injection was completed. Once the injection was complete, mice were placed on a heating pad until fully awake and returned to their primary housing facility. Each animal received 0.1cc/10g Ketofen subcutaneously once fully awake. All mice were individually housed post-op to allow healing. **Table 1** summarizes mice and treatment conditions. The treatment paradigm consisted of bilateral injections to caudate-putamen at 2 months and tissue harvest at 6 months.

Mouse tissue collection

At 6 months of age, Q7/Q7 WT or zQ175DN HD were deeply anesthetized with tribromoethanol (Avertin) before cervical dislocation. Whole brains were removed and frozen fresh at -80°C until use.

Tissue fractionation, SDS-PAGE, western blot analysis, and capillary gel electrophoresis,

Tissue from freshly sacrificed mice was processed as previously reported (Iuliano, Seeley et al., 2021). Briefly, both striata were dissected and homogenized in 10mM HEPES pH7.2, 250mM sucrose, 1mM EDTA + protease inhibitor tablet (complete, mini, EDTA-free, Roche) and 100 ul was removed as crude homogenate. Remaining homogenates were centrifuged at 2000xg, the supernatant (S1) was removed, and the crude nuclear pellet (P1) was resuspended in the same buffer. Protein concentration was determined using the Bradford method (BioRad kit). Equal amounts of protein (10 ug) were separated by SDS-PAGE using 3-8% Tris acetate gels (Criterion 26 wells, BioRad). Crude homogenates were transferred to nitrocellulose using the Transblot Turbo and P1 samples were transferred to PVDF using a

wet transfer overnight at 35V (Vodicka et al., 2014). After blocking in 5% milk/TBST, blots were incubated in primary antibody diluted in blocking buffer overnight at 4C. Antibodies and dilutions are as follows: Anti-HTT Ab1 (aa1-17, (DiFiglia et al., 1995), 1995, 1;2000, rabbit), Anti-HTT S830 (Generous gift of Dr. Gillian Bates, 1:6000, sheep), Anti-HTT MW8 (Developmental Studies Hybridoma Bank, University of Iowa, 1:500, mouse), PDE10a (Abcam, #ab177933, 1:2000, rabbit), SCN4B (Abcam, #ab80539, 1:750, rabbit), DARPP32 (Abcam, #ab40801, 1:8000, rabbit), GFAP (MilliporeSigma, #AB5804, 1:8000, Rabbit), Vinculin (MilliporeSigma, #V9131, 1:2000, mouse), GAPDH (MilliporeSigma, #MAB374, 1:10000, mouse). Blots were washed in TBST, incubated in secondary antibodies diluted in blocking buffer (Jackson ImmunoResearch1:2500 for rabbit, 1:5000 for mouse and sheep) for 1 hour at room temperature, washed, and bands were visualized using Super Signal West Pico Plus Chemiluminescent substrate (ThermoScienific) and CCD camera (AlphaInotech) or ChemiDoc XRS+ with Image Lab software (BioRad). Capillary For capillary gel electrophoresis the automated simple western system (Wes, ProteinSimple) was utilized to analyze equal amounts of protein (0.6 ug) with anti-polyQ antibody MW1 at a 1:50 dilution and Vinculin loading control at a 1:5000 dilution following manufacturer's standard protocol for the 66-440kD assay kit. Protein levels were determined from the electropherogram data using Compass for Simple Western software (ProteinSimple) where the peak area of mHTT was normalized to the peak area of vinculin for each mouse. Images in Figure 2B were acquired using the "lane view" option in the Compass software to mimic traditional western blots.

Filter trap assay

Aggregation assay was performed as previously reported (Weiss et al., 2008;Shing et al., 2023). Briefly, 40 ug P1 fraction was diluted to a final concentration of 2% SDS and vacuumed through a cellulose acetate membrane pre-equilibrated in 2% SDS using a dot blot apparatus (BioRad). Wells were washed with 2% SDS and the membrane was removed from the apparatus, washed in TBST then processed as for western blot as described above using anti-HTT antibodies S830 and MW8.

Pixel intensity quantification

Using ImageJ software, the area and average signal intensity of bands on western blot were determined by manually circling each band and multiplying to obtain the total signal intensity. For the P1 smear, the signal above the full length HTT band was measured. The total signal intensity for each protein was normalized to the vinculin or GAPDH loading controls. For the filter trap assay, the average signal intensity inside an equal size circle corresponding to the size of the well minus the background signal from an empty well was determined for each sample. Statistical analyses were unpaired t-test for mHTT levels by western blot and capillary electrophoresis and One-way ANOVA with Tukey's multiple comparison test for all other proteins and filter trap assay.

Lipid Extraction, LC-MS, and Annotations

Lipids were extracted using the two-phase methyl-*tert*-butyl ether (MTBE) method as previously described (Matyash et al., 2008). Briefly, 80 µl of crude homogenate from dissected mouse striatum in sucrose-HEPES buffer were transferred to 7 ml glass scintillation vials containing 750 µl of HPLC grade methanol. The vials were vortexed, then 2.5 ml of HPLC grade MTBE was added to each vial and incubated on a platform shaker for 1 hour. 625 µl of water was then added to induce phase separation. Samples were incubated for 10 minutes at room temperature, then centrifuged at 1,000g for 10 minutes. The lipid containing organic (upper) phase was transferred into a new vial, and the lower phase was

reextracted with 1 ml re-extraction solvent, obtained by collecting the upper phase of a mixture of MTBE/methanol/water in a 10:3:2.5, v/v/v ratio. The lipid containing upper phases were combined and dried under a stream of nitrogen at 35 ºC. Lipid extracts were resuspended in 35 µl of a 1:1 mixture of methanol and 2-propanol, and hand delivered to the Beth Israel Deaconess Mass Spectrometry Core. The lipid extracts were analyzed by positive/negative ion switching LC-MS/MS and annotated using LIPIDSearch as described (Breitkopf et al., 2017). Annotations are classified by LIPID MAPS subclasses.

Lipid Abbreviations

Glycerophospholipids: Bis-methyl phosphatidic acid (BisMePA), Dimethyl phosphatidylethanolamine (dMePE), Lysophosphatidylcholine (LPC), Lysophosphatidylethanolamine(LPE), Lysophosphatidylglycerol (LPG), Lysophosphatidylinositol (LPI), Lysophosphatidylserine(LPS), Lysodimethyl phosphatidylethanolamine (LdMePE), Methyl- Phosphatidyl Choline (MePC), Phosphatidic acid (PA), Phosphatidylcholine (PC), Phosphatidylethanolamine(PE), Phosphatidylethanol (PEt), Phosphatidylglycerol (PG), Phosphatidylinositol (PI), Phosphatidylinositol-monophosphate (PIP), Phosphatidylmethanol (PMe), Phosphatidylserine(PS). *Glycerolipids:* Diacylglyceride (DG), Monoacylglyceride (MG), Monogalactosyldiacylglycerol (MGDG), Monogalactosylmonoacylglycerol (MGMG), Triacylglyceride(TG). *Sphingolipids:* Dihexosylceramide (Hex2Cer), Ceramides (Cer), Ceramide phosphate (CerP), Ganglioside (GD1a, GD1b), Hexosylceramide (Hex1Cer), Simple Glc series (CerG2GNAc1), Sphingomyelin (SM), Sphingomyelin phytosphingosine (phSM), Sphingosine (SPH), Sulfatide (ST). *Sterols:* AcylGlcCholesterol ester (AcHexChE), Cholesterol Ester (ChE), Zymosterol (ZyE). *Fatty Acyls:* Acyl Carnitine (AcCa), Fatty Acid (FA), N-acylethanolamine (AEA), (O-acyl) -1-hydroxy fatty acid (OAHFA), Wax ester (WE). *Prenol lipids:* Coenzyme (Co).

Computational analysis/visualization

To correct for duplicate annotation of duplicate lipid ions by LipidSearch, due to their wide elution profiles, all instance of identical lipid ions were summed together. Lipid ions were then filtered using the LipidSearch parameter (Rej. = 0) and lipid ions missing in over 20% of the samples were excluded from analysis. Data was then log-transformed and normalized with Eigen MS (Karpievitch et al., 2014). The principal component analysis was performed using FactoMineR (v2.11), data was centered and scaled. Total level of lipid in each sample was determined by summing the intensity of all the lipid ions in each sample. The heatmap in figure 3 was generated in R using ComplexHeatmaps (v2.20.0; (Gu, 2022)). Each column represents data from one animal. Rows represent a lipid subclass with colors being assigned based on the minimum (blue) and maximum (red) expression of each subclass. Statistical significance of lipid subclasses was determined by one-way ANOVA between all 3 groups, followed by Tukey's t-test (p value), and the false discovery rate (FDR, 5%) (q value) was controlled by the two-stage linear step-up procedure of Benjamini, Krieger, and Yekutieli (lipid subclass N=42, lipid ions N=2398).

Somatic expansion index

Genomic DNA was isolated from striatal P1 samples (Qiagen DNEasy Blood and Tissue kit, Cat. 69504) and purified (New England Biolabs Monarch PCR and DNA Cleanup Kit, Cat. T1130) and average CAG number in HTT was determined by PCR and capillary gel electrophoresis of PCR products at the MGH Genomics Core. The starting (inherited) CAG for each mouse was provided by Jackson laboratories from tail DNA. Expansion Index was calculated as described, using a custom Python script. (Lee et al., 2010).

Results

Lowering of mutant HTT protein in Q175DN HD mice

To test whether a gene therapy capable of allele-specific gene repression could prevent lipid-related neurodegenerative changes in an HD preclinical mouse model, prepared virus for AAV9-ZFP-HTT or AAV9-ZFP-dDBD (**Figure 1B**) were introduced into the zQ175DN HD mouse caudate-putamen with bilateral injections at two months of age, prior to few known behavioral phenotypes in this model (Peng et al., 2016;Koch et al., 2024). Wild-type (WT) mice were injected with AAV9-ZFP-dDBD virions as an additional control to obtain baseline levels of genotype-dependent changes in proteins and lipids. All tissues were harvested at six months of age when considerable changes in transcription have been described in zQ175/Q7 striatum compared to WT, nuclear and cytoplasmic aggregates are present and electrophysiological changes can be detected (Langfelder et al., 2016;Zeitler et al., 2019)).

To examine HTT protein levels, we performed capillary gel electrophoresis on crude homogenates of AAV-treated caudate-putamen of zQ175DN HD mice using anti-polyglutamine antibody, MW1, to detect mutant HTT protein (mHTT). Results showed a significant lowering (48%) of mHTT with expression of ZFP-HTT but not with ZFP-dDBD in caudate-putamen of HD mice (**Figure 2A and B**). We also performed western blot (WB) assays using the crude homogenates from both WT and HD treated mice and probed with anti-N-terminal HTT antibody Ab1, which detects both WT HTT and mHTT (**Fig 2C and D**, (DiFiglia et al., 2007;Sapp et al., 2020;Shing et al., 2023)). Using this method, pixel intensity quantification showed that the level of mHTT was 43% lower in the zQ175/Q7 HD mice treated with ZFP-HTT compared to those treated with ZFP-dDBD (**Fig 2D**). The levels of WT HTT were an average of 54 and 64% lower in zQ175DN HD WT mice with two WT alleles, as expected (**Fig 2D**). There was no difference in WT HTT levels between the zQ175/Q7 treatment groups demonstrating the specificity of the ZFP-HTT repressor protein for the mutant HTT allele. Thus, four months after injection, mHTT in crude homogenates was significantly lowered with ZFP-HTT treatment compared to the control virus (HTT-dDBD) and WT HTT levels were spared.

A molecular species of mHTT persists with lowering by ZFP-HTT.

Previously, we showed that a molecular species of mHTT in the crude nuclear pellet fraction (P1) was resistant to lowering in LacQ140 mice (Shing et al., 2023). We and others have shown that the anti-HTT antibody S830 detects a slowly migrating species of mHTT that appears as a high molecular weight smear in homogenates from brain tissues containing mHTT (Landles et al., 2010;Vodicka et al., 2014;Shing et al., 2023). Using Ab1 on WB, levels of mHTT were 54% lower in P1 from zQ175DN mice treated with ZFP-HTT compared to ZFP-dDBD (**Fig 3A, B**). WT HTT levels in the P1 fraction were an average of 50-53% lower in the zQ175DN mice compared to Q7/Q7, as expected for one allele versus two alleles of normal HTT, consistent with findings above in crude homogenates. However, whereas antibody S830 recognized full-length soluble mHTT detected as a resolvable band which was 44% lower in the AAV9-HTT-ZFP mice compared to those treated with AAV9-HTT-dDBD, no lowering of the high molecular weight smear occurred (**Fig 3A, C**). This result is consistent with our findings in LacQ140 striatum where a S830-positive species of misfolded HTT persists even with transcriptional lowering. Next, a filter trap assay to analyze lowering of aggregated mHTT in P1 was employed. MW8 antibody, which detects aggregated exon1 HTT (Landles et al., 2010), showed a significant reduction of aggregated

mHTT in the zQ175DN mice treated with AAV9-HTT-ZFP compared to those treated with AAV9-ZFP-dDBD (**Fig 3D**).

All together, these data indicate that reducing mutant *HTT* transcription with AAV9-HTT-ZFP lowers soluble and aggregated forms of mHTT in crude homogenate and P1 fraction, but that a S830-positive misfolded molecular species of mHTT which is present in the crude nuclear fraction resists lowering.

Effects of AAV9-ZFP-HTT on other proteins known to be affected in HD

To determine if intrastriatal injection of AAV9-ZFP-HTT affects levels of other proteins, we performed WB analysis of four proteins shown to be affected in HD mouse models (Valencia et al., 2013;Sapp et al., 2020). Loss of PDE10 is an early change in most HD mouse models including zQ175/Q7 (Zeitler et al., 2019;Sapp et al., 2020). PDE10 was reduced in the zQ175DN mice treated with the control virus AAV9-HTT-dDBD compared to Q7/Q7 mice injected with AAV9-HTT-dDBD (**Figure 4**). However, even with significant lowering of mHTT (48 and 43%, *Figures 2A and B*), the levels of PDE10 were not affected in the zQ175DN mice in AAV9-ZFP-HTT transduced mice (**Figure 4**). In this experiment, the levels of SCN4B, GFAP and DARPP32 were not yet changed between the Q7/Q7 and zQ175DN mice at six months (**Figure 4**).

Treatment with AAV9-ZFP-HTT prevents genotype-dependent lipid changes in Q175DN HD mice.

Previously, we found that age and genotype dependent lipid changes occur in both zQ175/Q7 mice (Iuliano et al., 2021) and LacQ140 mice, and these changes could be prevented by early whole body genetic downregulation of mutant *HTT* transcription in LacQ140 mice (Shing et al., 2023). To test whether intrastriatal injection of a therapeutic would have the same protective effects, we surveyed lipids in crude homogenates of our AAV-treated mice by liquid chromatography and mass spectrometry (LC-MS). LC-MS analysis of lipids from caudate-putamen of treated WT and zQ175DN mice at six months of age yielded high coverage of lipids species with 2,398 unique lipid ions identified across 42 lipid subclasses. To assess the variation within the data, a principal component analysis (PCA) was performed. The projection of the two most informative principal components, PC1 and PC2 are shown in **Fig 5A** (PC1, 13.7% of variance; PC2, 8.3% of variance). WT Q7/Q7 mice treated with the control virus (AAV9-ZFP-dDBD), zQ175DN HD mice treated with control virus (AAV9-ZFP-dDBD), and zQ175DN HD mice treated with the therapeutic virus (AAV9-ZFP-HTT) separated into their own groups along the first principal component (white circles, dark green triangles, light green circles, respectively), with zQ175DN HD mice treated with the therapeutic arm moving closer to the WT mice treated with control virus. On the second principal component zQ175DN HD mice regardless of treatment separated from Q7/Q7 WT mice treated with the control virus disclosing a genotypic difference unaffected by therapy. To confirm the PCA results obtained using two components, we undertook a more in-depth quantitative analysis called k-means computational clustering, which considers changes in all lipid levels (increased or decreased). We queried which two of the groups (k=2) were similar using this method with 25 initial starting points employed on the first eight principal components which accounted for 51% of the total variation. zQ175DN HD mice treated with the control virus clustered into group A (**Figure 5A, *blue ellipse***) and Q7/Q7 WT mice treated with the AAV9-ZFP-dDBD and zQ175DN mice treated with AAV9-ZFP-HTT clustered into group B (**Figure 5A, *red ellipse***). This k-cluster analysis showed that HD mice that had received the therapeutic were more similar to WT mice than HD mice that had received the control virus.

An examination of total lipid levels showed a genotype-dependent loss of lipids in HD mouse caudate-putamen (25-30%) compared to WT mice treated with control virus (**Fig 5B**), consistent with previous results in LacQ140 mice. One-way ANOVA revealed significant differences in total lipid levels. zQ175DN HD mice treated with the AAV9-ZFP-dDBD had 25-30% lower levels of lipids than both Q7/Q7 WT mice treated with the AAV9-ZFP-dDBD and zQ175/Q7 HD mice treated with AAV9-ZFP-HTT (**Fig 5B**). Of note, there was no significant difference between Q7/Q7 WT mice treated with control virus (AAV9-ZFP-dDBD) and zQ175DN HD mice treated with AAV9-ZFP-HTT. These data show that lowering mHTT levels preserved total lipid levels in treated HD mice.

When examined by lipid subclass, we found changes in most lipid subclasses were prevented by treatment with AAV9-ZFP-HTT. There were 22 subclasses of lipids that were significantly lower in zQ175DN HD mice treated with AAV9-ZFP-dDBD compared to Q7/Q7 WT mice treated with AAV9-ZFP-dDBD (**Fig 5C and Supplementary Fig1**). In 90.9% (20/22) of those subclasses, there was no significant difference between Q7/Q7 WT mice treated with AAV9-ZFP-dDBD and zQ175DN HD mice treated with AAV9-ZFP-HTT (**Fig 5C**). Interestingly, the sphingolipids, sphingomyelin, and ceramide were significantly higher in zQ175DN mice treated with AAV9-ZFP-HTT than zQ175DN and Q7/Q7 mice treated with AAV9-ZFP-dDBD (**Supplementary Fig1**).

Individual lipid species can have precise functions in signaling such as arachidonic acid signaling (Zhang et al., 2023) and myelin stability (Alderson et al., 2006;Zhang et al., 2023) (**Supplementary file 1**). AAV9-ZFP-HTT treatment prevented most genotype-dependent changes in individual lipid species. When compared to Q7/Q7 WT mice treated with the control virus, the zQ175DN HD mice treated with the control virus had 260 of 2,398 significantly altered individual lipid ions. Of those, 93% (242/260) were not significantly different for zQ175DN HD mice treated with AAV9-ZFP-HTT compared to Q7/Q7 WT mice treated with AAV9-ZFP-dDBD **(Table 2**), demonstrating outstanding protection against lipid deterioration by the therapeutic. However, while phosphatidylserine (PS) was not significantly altered as a subclass, 28/170 individual species were significantly different between Q7/Q7 WT mice and zQ175DN HD mice both treated with AAV9-ZFP-dDBD (**Supplementary File 1**). AAV9-ZFP-HTT treatment also introduces some new changes to levels of lipids. There were 117 lipid species that were only significantly different between Q7/Q7 WT mice both treated with control vector and zQ175DN HD mice treated with AAV9-ZFP-HTT. Notably, while there was only one significantly altered triacylglyceride (TG) lipid ion between Q7/Q7 WT mice and zQ175DN HD mice treated with AAV9-ZFP-dDBD, there were 15 TG lipid ions significantly altered between Q7/Q7 WT mice treated with control vector and zQ175DN HD mice treated with AAV9-ZFP-HTT (**Supplementary File 1**).

These data show that therapeutic lowering with AAV9-ZFP-HTT is highly effective at protecting HD mice from most degenerative changes in lipids. Changes in individual lipids indicate introduction of the AAV vectors has effects on specific species independent of mHTT levels.

Discussion

In this study we found numerous changes in lipid species between WT and zQ175DN HD mice at six months of age, and preservation of levels for most lipids with intrastriatal injection of a lowering therapy. We also detected a misfolded species of mHTT resistant to lowering present in the crude nuclear fraction, reproducing earlier results in a different mouse HD model. Our results show that LC-MS offers a

quantitative way to track biochemical changes in lipids reflective of neurodegeneration in preclinical models.

Treatment with AAV9-ZFP-HTT resulting in mHTT lowering was highly effective at preventing lipid changes in caudate-putamen of zQ175DN mice. Thus, while complete reversal of all pathologies, including transcriptional changes, may require either very early mHTT lowering, targeting existing mHTT in nuclear compartments, or interventions targeting other mechanisms such as somatic instability, lowering mHTT with AAV9-ZFP-HTT still awarded significant benefits as measured by lipid changes.

Many of the lipid changes found in zQ175DN mice in this study were like those found in synaptic fractions in zQ175/Q7 mice at six months of age in our previous study (Iuliano et al., 2021). Lipid changes in the LacQ140 mice, which have a shorter CAG repeat and a more prolonged disease process, were slightly different and changed with age, but also showed a significant loss of total lipids (at 9 months) with heavy losses of lipids important for white matter. Here, we also saw loss of lipids important for white matter health (SM, Hex2Cer, sulfatides), which can be lost with neurodegeneration and aging (Blomqvist et al., 2021;Dimovasili et al., 2024), but lipid profiles were unique to each animal model. The identity of lipids changed in HD mice (measured by us) and measured in HD autopsy tissue (Phillips et al., 2022) are consistent with altered white matter, which reflects processes observed in HD patients and is likely to affect nerve conduction (reviewed by (Sun et al., 2022). Allele specific lowering of mHTT with AAV9-ZFP-HTT rendered lipid profiles at the subclass level virtually unchanged in zQ175DN mice compared to WT mice treated with a control virus, an indication of efficacy of the treatment. The small number of specific lipids changed was dependent on both the genotype and the cDNA insert expressed from the AAV, but overt signs of toxicity were not observed in any of the treatment groups.

We found a molecular species of mHTT present in the crude nuclear fraction and resistant to lowering, reproducing our earlier findings (Shing et al., 2023). In HD models, PDE10 mRNA and protein levels are downregulated (Hebb et al., 2004) as part of a profound transcriptomic pathology affecting numerous genes (Luthi-Carter et al., 2000;Langfelder et al., 2016). Global gene repression may be due to the presence of a misfolded form of mHTT in the nucleus first described by Wheeler et al. (Wheeler et al., 2000), direct binding to DNA and repression (Kegel et al., 2002;Benn et al., 2008), or through sequestration of transcriptional activators and repressors (Boutell et al., 1999;Steffan et al., 2000;Dunah et al., 2002;Zuccato et al., 2003). Partial gene repression of the mutant *HTT* allele initiated at embryonic day five relieved repression of PDE10 and partially corrected a wider transcriptomic pathology in LacQ140 mice (Marchionini et al., 2022). In contrast, we did not see a rescue of PDE10 levels in the current study. Initiating lowering at two months (both in this study and in one arm of the LacQ140 study) appears to allow for accumulation of a toxic form of mHTT, which resists lowering and disturbs transcription. Another possibility is that the LacO repressor system in LacQ140 mice repressed mHTT in all brain regions and cell types (neurons and glia types) as well as peripheral tissues, providing greater benefit. The AAV1/2 expressing ZFP-HTT used by Zeitler et al. was directly injected into the striatum and had a human synapsin promotor, thus limiting expression to neurons had a modest effect on PDE10 (Zeitler et al., 2019). For this study we used a chicken beta-actin promotor which should drive expression in both neurons and glia but still saw no benefit for PDE10. These data suggest that once the HD transcriptomic phenotype is established it is difficult to reverse, even with transcriptional lowering of mutant *HTT* which also blocks HTT1a expression.

Cross referencing lipidomic data with transcriptomic data revealed that some but not all changes in lipid levels could be explained by transcriptional changes of enzymes related to their production or turnover. Nevertheless, significant protection from lipid changes with mHTT lowering occurred despite

only about 50% recovery of transcriptional changes (Shing et al., 2023). mHTT immunoreactivity can be detected with PHP1 and PHP2 in myelin in zQ175/Q7 mice (Ko et al., 2018) positioning mHTT to contribute to pathology through post-transcriptional mechanisms such as interfering with membrane-associated protein complexes or changing lipid bilayer organization through direct lipid-mHTT interactions (Kegel et al., 2005;Suopanki et al., 2006;Atwal et al., 2007). However, the impact of mHTT in these compartments can be achieved by lowering.

Carroll and colleagues (Mathews et al., 2024) reported that binding of ZFP-HTT to the CAG on the HTT allele may block somatic instability providing additional protection from disease in addition to that afforded by mHTT protein lowering. A CAG repeat of 175 is thought to already exceed the length needed to induce most phenotypes including transcriptional phenotypes without further expansion (Aldous et al., 2024). Even so, in addition to lowering mHTT levels, impeding somatic instability with ZFP-HTT may be one mechanism that contributes to the protection of lipid levels in our study.

In conclusion, assessment of lipid levels using a quantitative method revealed sweeping positive effects of a lowering therapeutic targeting mutant HTT transcription in a preclinical mouse model of HD.

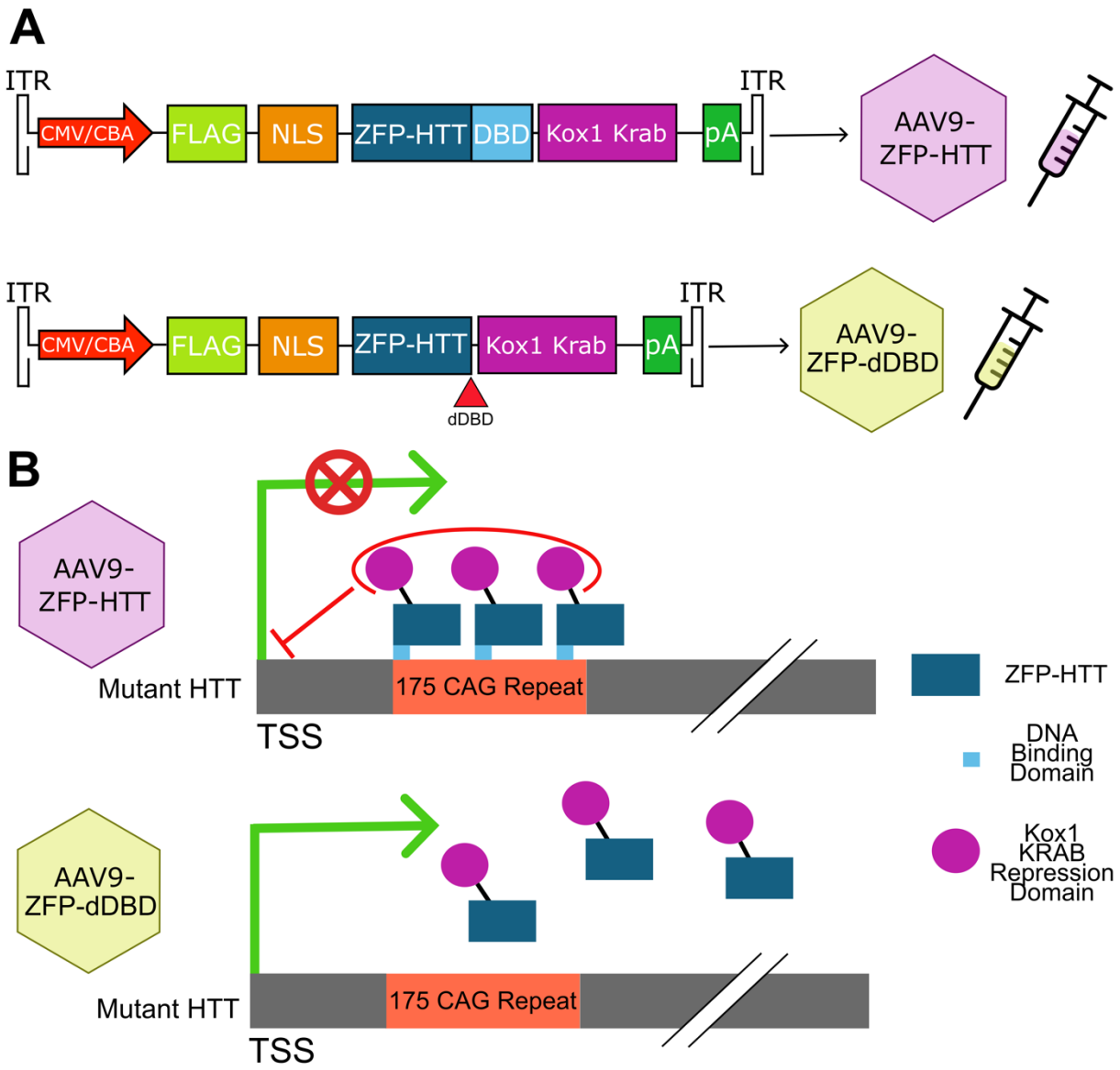

Figure 1. Diagram of AAV9-HTT-ZFP and AAV9-ZFP-dDBD constructs.

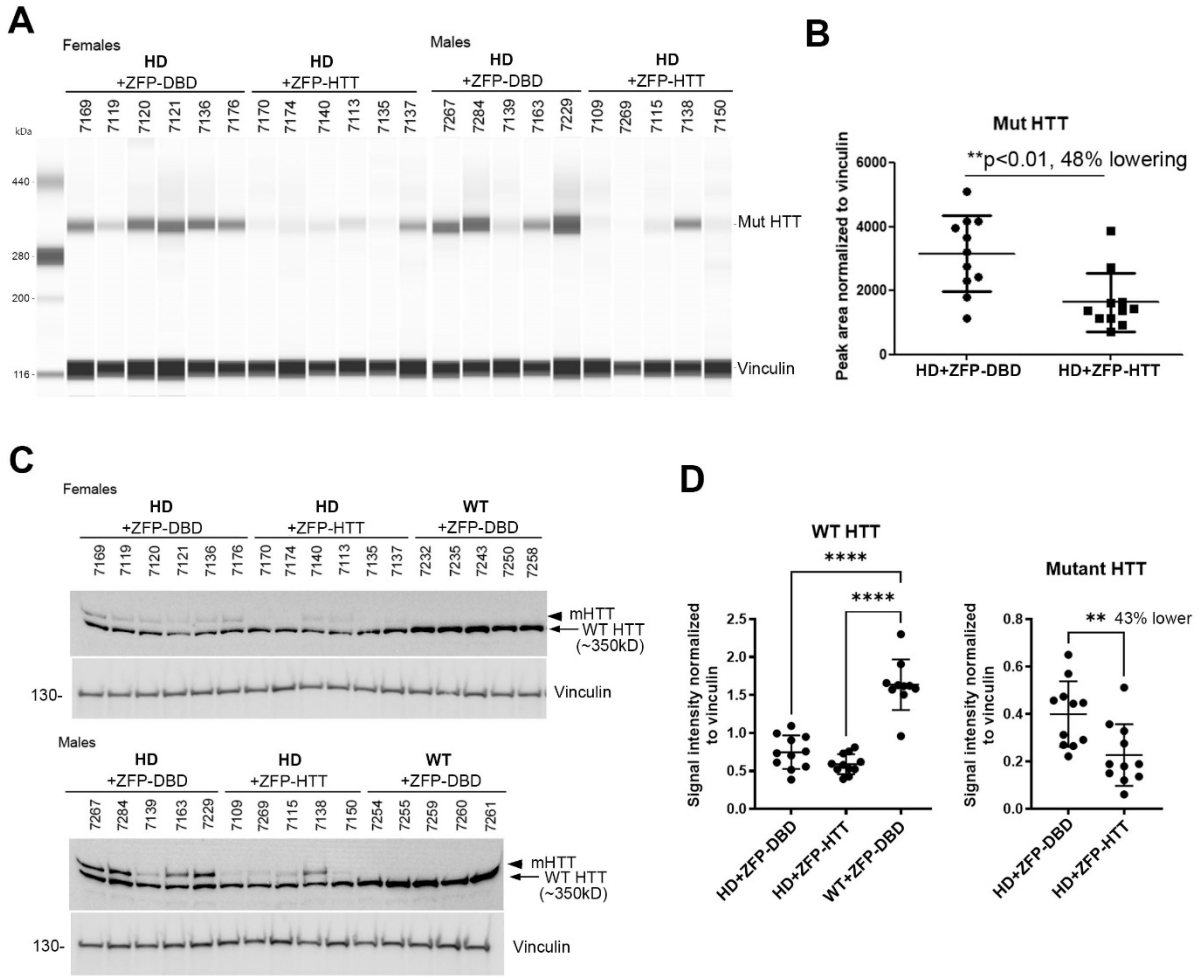

Figure 2. Capillary electrophoresis (WES) analysis and western blot analyses of protein levels of soluble normal and mutant Huntingtin in crude homogenates from zQ175 caudate-putamen injected with AAV9-ZFP-HTT or AAV9-ZFP-dDBD and WT injected with AAV9-ZFP-dDBD.

A. Lane view image of automated simple western (Wes) using equal amounts of protein (0.6ug) and anti-polyQ antibody MW1. B. Quantification of capillary electrophoresis shows significant lowering of mutant HTT by 48% with ZFP-HTT treatment compared to treatment with ZFP-DBD in Q175/Q7 HD mice. **C**. Western blot images show equal protein loading (10 ug) of crude homogenates from female (top) and male (bottom) mice probed with antibodies indicated to the right of the blots. **D.** Graphs show signal intensity normalized to vinculin of the combined female and male samples. There is significantly less WT HTT in the Q175/Q7 HD mice compared to WT mice, as expected (50-60% less, ****p<0.0001, One-way ANOVA with Tukey's multiple comparison test, n=10-11 per group). There is 43% lowering of mutant HTT in the ZFP-HTT treated Q175 HD mice compared to the ZFP-DBD treated HD mice (**p<0.01, unpaired t test, n=11 per group).

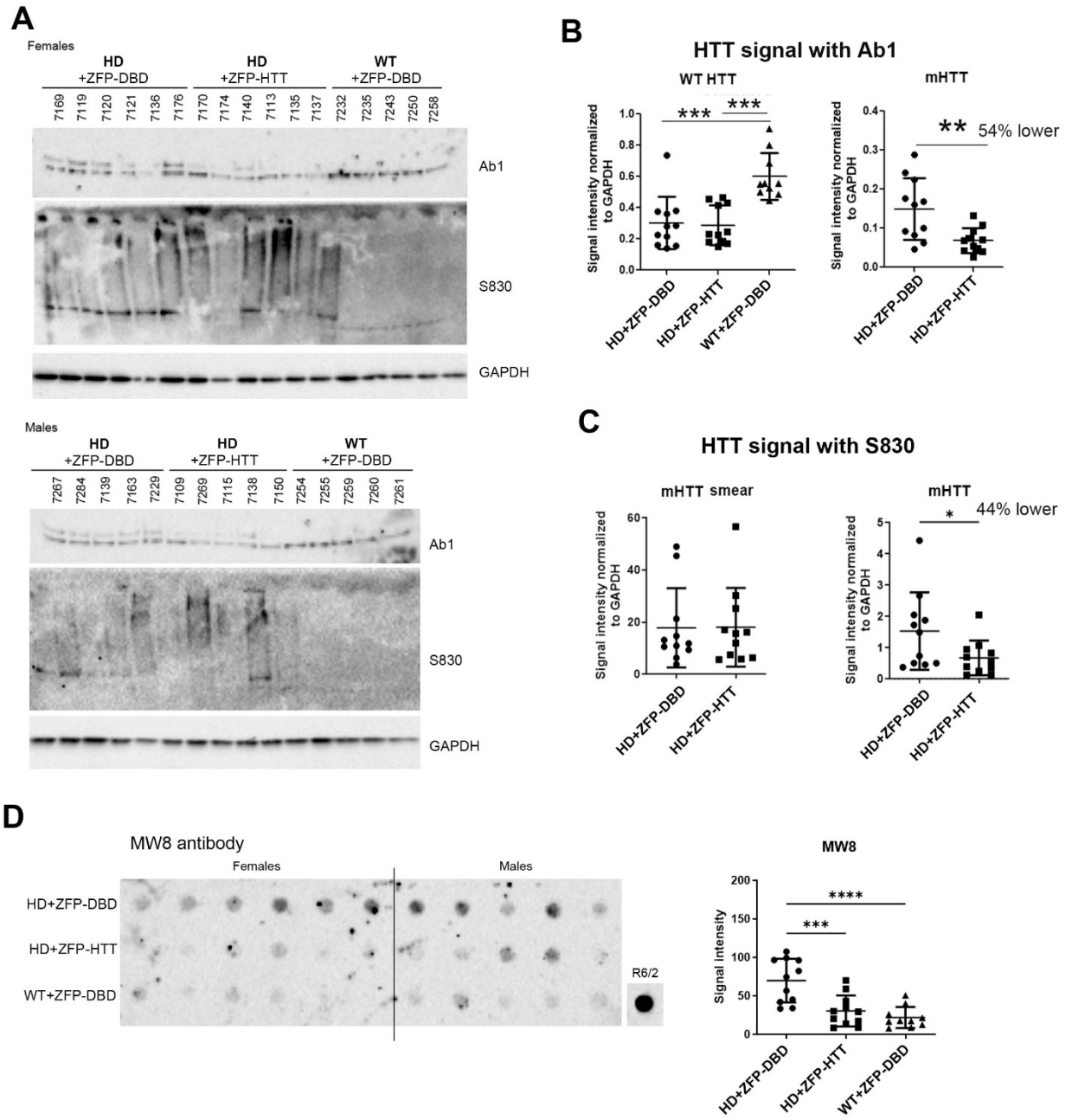

Figure 3. Protein analysis of the crude nuclear P1 fractions from caudate-putamen from mice injected with AAV9-ZFP-HTT or AAV9-ZFP-DBD and WT injected with AAV9-ZFP-dDBD analyzed by western blot and gel filtration.

A. Equal amounts of protein (10ug) from the P1 fractions were separated by SDS-PAGE and probed with anti-HTT antibody S830 to detect SDS-resistant high molecular weight HTT protein. Another gel was run with the same samples and probed with anti-HTT antibody Ab1 to detect full-length soluble HTT. **B, C.** No significant difference aggregated HTT in the smear at the top of the gel with S830 was detected in the Q175/Q7 mice treated with ZFP-DBD or ZFP-HTT but there was significant lowering of full-length HTT as detected with Ab1 (54% lower, **p=0.0056, unpaired t test) and S830 (44% lower, *p=0.0494, unpaired t test) in the P1 fraction similar to we saw in the crude homogenates. **D.** Filter trap assay using

40ug samples of the P1 fraction with MW8 antibody shows significantly more aggregated HTT protein on the membrane in HD+ZFP-DBD mice compared to both HD+ZFP-HTT and WT+ZFP-DBD mice and no difference between HD+ZFP-HTT and WT+ZFP-DBD mice (One-way ANOVA with Tukey's multiple comparison test, ***$p<0.001$, ****$p<0.0001$).

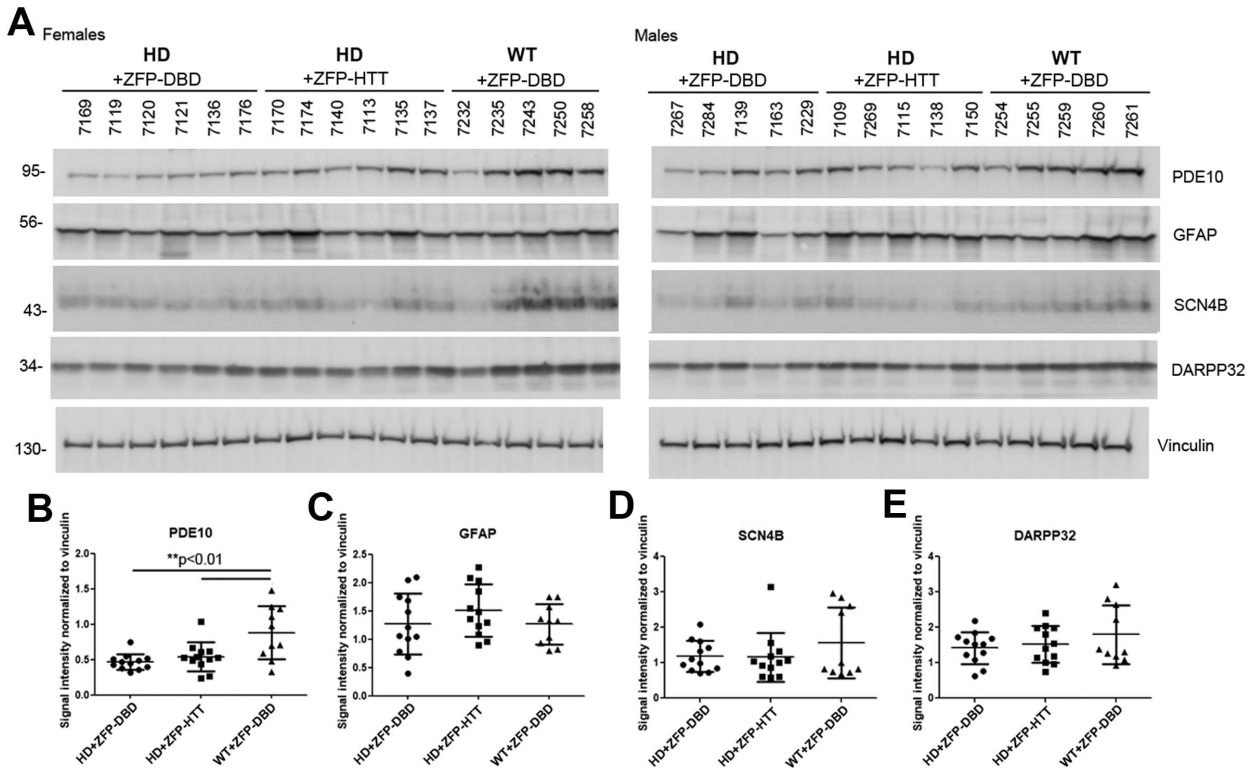

Figure 4. Western blot analyses of PDE10, SCN4b, GFAP, and DARPP32 in crude homogenates from zQ175 caudate-putamen injected with AAV9-ZFP-HTT or AAV9-ZFP-dDBD and WT injected with AAV9-ZFP-dDBD.

A. Western blot images show equal amounts of protein (10ug) from Q175/Q7 HD mice treated with ZFP-DBD or ZFP-HTT or WT mice treated with ZFP-DBD probed with antibodies to PDE10, GFAP, SCN4B and DARPP32. The molecular weight markers are indicated on the left of the blots. **B**. There was significantly less PDE10 in the Q175/Q7 HD mice compared to the WT mice but the level did not reverse with 43% mHTT lowering (**p<0.01, One-way ANOVA with Tukey's multiple comparison test, n=10-11 per group). There were no differences in the levels of GFAP (**C**), SCN4B (**D**) or DARPP32 (**E**) between the Q175/Q7 HD and WT mice.

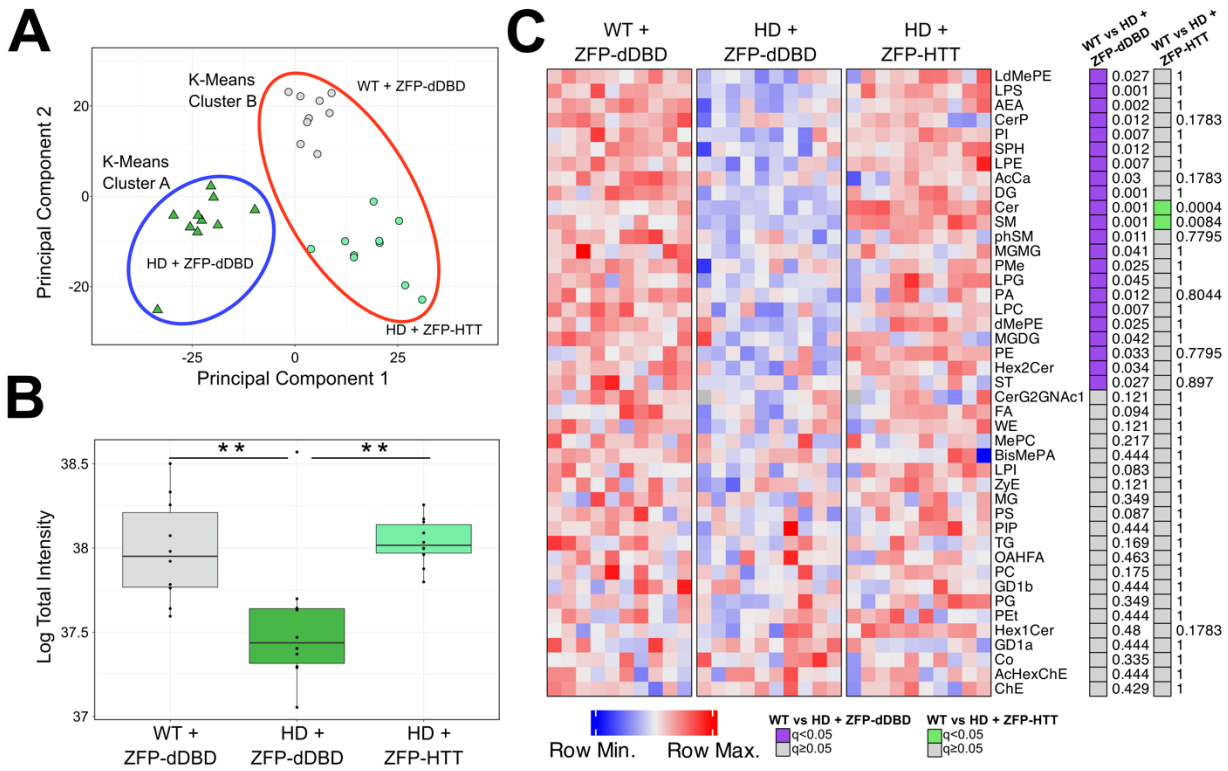

Figure 5: Protection of total lipid levels and subclass levels via lowering of mutant HTT. **(A)** Unsupervised classification methods showed prevention of lipid changes by lowering of mutant HTT. The 1st principal component captured 13.7% of variation and showed Q7/Q7-ZFP-dDBD (white circles) mice cluster closer to Q175/Q7-ZFP-HTT (light green circles) mice than Q175/Q7-ZFP-dDBD (dark green triangle) mice. The second principal component captured 8.33% of variation and the Q7/Q7 WT mice separated from both Q175/Q7 treatment groups. *K-means clustering*, with k = 2, and 25 different initial start points clustered all the Q7/Q7-ZFP-DBD and Q175/Q7-ZFP-HTT together (Cluster B, red ellipse) and clustered Q175/Q7-ZFP-DBD points separately (Cluster A, blue ellipse). Taken together this indicates that lowering of mutant HTT can prevent many lipid changes in HD. **(B)** Loss of total lipid intensity is prevented by lowering of mutant HTT. One way ANOVA revealed significant differences in total lipid levels. ($F(2,27) = 7.822$; $p = 0.00209$). zQ175/Q7 mice treated with the AAV9-ZFP-dDBD had 25-30% lower levels of lipids than both Q7/Q7 WT mice treated with the AAV9-ZFP-dDBD ($p = 0.00879$) and zQ175/Q7 HD mice treated with AAV9-ZFP-HTT ($p = 0.00357$). **(C)** Lowering of mutant HTT prevents changes in many subclasses. The heatmap depicts individual animals (columns) and lipid subclass intensities (rows). WT vs HD+ZFP-DBD column indicates lipid subclasses significantly different between WT and HD mice treated with the control vector (purple boxes, $q<0.05$; One-way ANOVA with Tukey's multiple comparison test, two-stage linear step-up procedure of Benjamini, Krieger and Yekutieli, N=42 lipid subclasses, n=10 mice). WT vs HD+ZFP-HTT column indicates lipid subclasses significantly different between WT and HD mice treated with AAV9-ZFP-HTT (green boxes, $q<0.05$; One-way ANOVA with Tukey's multiple comparison test, two-stage linear step-up procedure of Benjamini, Krieger and Yekutieli, N=42 lipid subclasses, n=10 mice).

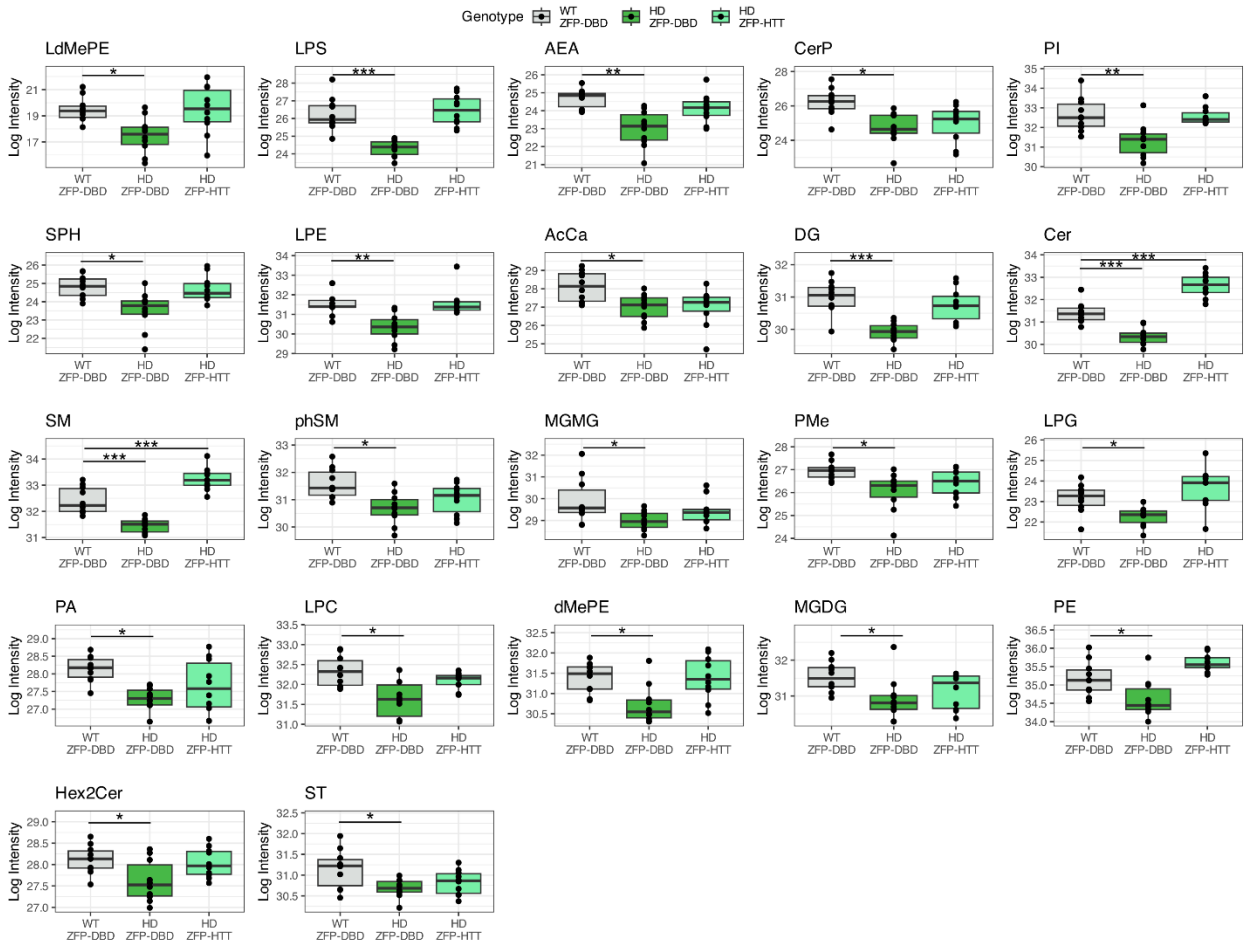

<u>Supplemental Figure 1: Significantly altered lipid subclasses in caudate-putamen of 6 month mice.</u> Graphs shown mean and interquartile ranges of significantly altered lipids. All data was analyzed via One-Way ANOVA with Tukey's multiple comparisons test and all multiple comparisons were corrected with two-stage linear step-up procedure of Benjamini, Krieger and Yekutieli, N=42 lipid subclasses, n=10 mice; *q<0.05, ** q<0.01, ***q<0.001). *LdMePE:* (F(2,27)=6.167, p = 0.00622; Tukey's between WT and HD treated with control vector q= 0.0266). *LPS*: (F(2,27)=22.6, p=0.00000171; Tukey's between WT and HD treated with control vector q=0.0008). *AEA:* (F(2,27)=11.4, p=0.000258; Tukey's between WT and HD treated with control vector q=0.0016). *CerP:* (F(2,27)=7.218, p=0.00308; Tukey's between WT and HD treated with control vector q=0.0120). *PI:* (F(2,27)=5.011, p=0.0141; Tukey's between WT and HD treated with control vector q=0.0067). *SPH:* (F(2,27)7.687, p=0.00228; Tukey's between WT and HD treated with control vector q=0.012). *LPE:* (F(2,27)=11.58, p=0.000233; Tukey's between WT and HD treated with control vector q=0.0067). *AcCa:* (F(2,27)=5.924, p=0.00736; Tukey's between WT and HD treated with control vector q=0.0298). *DG:* (F(2,27)=5.53, p=0.0000325; Tukey's between WT and HD treated with control vector q=0.0008). *Cer:* (F(2,27)=60.1, p=0.000000000114; Tukey's between WT and HD treated with control vector q=0.0008, WT and HD-ZFP-HTT q=0.0004). *SM:* (F(2,27)=46.13, p=0.00000000195; Tukey's between WT and HD treated with control vector q=0.0008, WT and HD-ZFP-HTT q=0.0084). *phSM:* (F(2,27)=6.859, p=0.0039; Tukey's between WT and HD treated with control vector q=0.0114). *MGMG:* (F(2,27)=3.709, p=0.0377; Tukey's between WT and HD treated with control vector q=0.0410). *PMe:* (F(2,27)= 5.002, p = 0.0142; Tukey's between WT and HD treated with control vector q=0.0253). *LPG:* (F(2,27)= 8.491 p = 0.00138; Tukey's between WT and HD treated with control vector q=0.0455). *PA:* (F(2,27)= 6.588, p = 0.00468; Tukey's between WT and HD treated with control vector q=0.0120). *LPC:* (F(2,27)= 8.17, p = 0.00168; Tukey's between WT and HD treated with

control vector q=0.0067). *dMePE:* (F(2,27)= 6.587, p = 0.00468; Tukey's between WT and HD treated with control vector q=0.0253). *MGDG:* (F(2,27)= 3.715, p =0.0376 ; Tukey's between WT and HD treated with control vector q=0.0421). *PE:* (F(2,27)= 11.58, p = 0.000077; Tukey's between WT and HD treated with control vector q=0.0331). *Hex2Cer:* (F(2,27)= 4.792, p = 0.0166; Tukey's between WT and HD treated with control vector q=0.0343). *ST:* (F(2,27)= 4.856, p = 0.0158; Tukey's between WT and HD treated with control vector q=0.0272).

Table 1. Mice and treatment groups

Mouse Genotype	AAV	Titer (vg/ml)	Injection Volume	Animal Number
Q7/Q7 WT	scAAV9-CB-ZFP^{DBD}	7 x 10 ^{12}	5 µl	10 (5F + 5M)
Q175/Q7 HD	scAAV9-CB-ZFP^{DBD}	7 x 10 ^{12}	5 µl	11 (6F + 5M)
Q175/Q7 HD	scAAV9-CB-ZFP^{Htt}	7 x 10 ^{12}	5 µl	11 (6F + 5M)

Table 2. Summary of individual lipid ions detected.

# Detected Lipid Ions	# Lipid Ions changed WT vs HD-ZFP-dDBD	# Lipid Ions Protected	# Novel Lipid Ion changed WT vs HD-ZFP-HTT
2398	260	242	117

All data was analyzed by One-Way ANOVA with Tukey's Multiple Comparisons and corrected by the two-stage linear step-up procedure of Benjamini, Krieger, and Yekutieli (N=2398). *Protected:* WT vs HD-ZFP-dDBD $q<0.05$ and WT vs HD-ZFP-HTT $q>=0.05$.
Novel Change: WT vs HD-ZFP-dDBD $q>= 0.05$ and HD-ZFP-HTT $q<0.05$

Supplementary Data:

File 1. Excel file containing LC-MS results for all individual lipids % intensities p values, q values. Statistical analysis performed by ANOVA and posthoc Tukey's test with 5% FDR correction.

References

(1993). A novel gene containing a trinucleotide repeat that is expanded and unstable on Huntington's disease chromosomes. The Huntington's Disease Collaborative Research Group. *Cell* 72**,** 971-983.

Alcala-Vida, R., Seguin, J., Lotz, C., Molitor, A.M., Irastorza-Azcarate, I., Awada, A., Karasu, N., Bombardier, A., Cosquer, B., Skarmeta, J.L.G., Cassel, J.C., Boutillier, A.L., Sexton, T., and Merienne, K. (2021). Age-related and disease locus-specific mechanisms contribute to early remodelling of chromatin structure in Huntington's disease mice. *Nat Commun* 12**,** 364.

Alderson, N.L., Maldonado, E.N., Kern, M.J., Bhat, N.R., and Hama, H. (2006). FA2H-dependent fatty acid 2-hydroxylation in postnatal mouse brain. *J Lipid Res* 47**,** 2772-2780.

Aldous, S.G., Smith, E.J., Landles, C., Osborne, G.F., Canibano-Pico, M., Nita, I.M., Phillips, J., Zhang, Y., Jin, B., Hirst, M.B., Benn, C.L., Bond, B.C., Edelmann, W., Greene, J.R., and Bates, G.P. (2024). A CAG repeat threshold for therapeutics targeting somatic instability in Huntington's disease. *Brain* 147**,** 1784-1798.

Alterman, J.F., Godinho, B., Hassler, M.R., Ferguson, C.M., Echeverria, D., Sapp, E., Haraszti, R.A., Coles, A.H., Conroy, F., Miller, R., Roux, L., Yan, P., Knox, E.G., Turanov, A.A., King, R.M., Gernoux, G., Mueller, C., Gray-Edwards, H.L., Moser, R.P., Bishop, N.C., Jaber, S.M., Gounis, M.J., Sena-Esteves, M., Pai, A.A., Difiglia, M., Aronin, N., and Khvorova, A. (2019). A divalent siRNA chemical scaffold for potent and sustained modulation of gene expression throughout the central nervous system. *Nat Biotechnol* 37**,** 884-894.

Atwal, R.S., Xia, J., Pinchev, D., Taylor, J., Epand, R.M., and Truant, R. (2007). Huntingtin has a membrane association signal that can modulate huntingtin aggregation, nuclear entry and toxicity. *Hum Mol Genet* 16**,** 2600-2615.

Batista, A. R., King, O. D., Reardon, C. P., Davis, C., Shankaracharya, Philip, V., Gray-Edwards, H., Aronin, N., Lutz, C., Landers, J., & Sena-Esteves, M. (2020). *Ly6a* Differential Expression in Blood-Brain Barrier Is Responsible for Strain Specific Central Nervous System Transduction Profile of AAV-PHP.B. *Human gene therapy*, *31*(1-2), 90–102.

Benn, C.L., Sun, T., Sadri-Vakili, G., Mcfarland, K.N., Dirocco, D.P., Yohrling, G.J., Clark, T.W., Bouzou, B., and Cha, J.H. (2008). Huntingtin modulates transcription, occupies gene promoters in vivo, and binds directly to DNA in a polyglutamine-dependent manner. *J Neurosci* 28**,** 10720-10733.

Blomqvist, M., Zetterberg, H., Blennow, K., and Mansson, J.E. (2021). Sulfatide in health and disease. The evaluation of sulfatide in cerebrospinal fluid as a possible biomarker for neurodegeneration. *Mol Cell Neurosci* 116**,** 103670.

Boutell, J.M., Thomas, P., Neal, J.W., Weston, V.J., Duce, J., Harper, P.S., and Jones, A.L. (1999). Aberrant interactions of transcriptional repressor proteins with the Huntington's disease gene product, huntingtin. *Hum Mol Genet* 8**,** 1647-1655.

Breitkopf, S.B., Ricoult, S.J.H., Yuan, M., Xu, Y., Peake, D.A., Manning, B.D., and Asara, J.M. (2017). A relative quantitative positive/negative ion switching method for untargeted lipidomics via high resolution LC-MS/MS from any biological source. *Metabolomics* 13.

Carroll, J.B., Warby, S.C., Southwell, A.L., Doty, C.N., Greenlee, S., Skotte, N., Hung, G., Bennett, C.F., Freier, S.M., and Hayden, M.R. (2011). Potent and selective antisense oligonucleotides targeting single-nucleotide polymorphisms in the Huntington disease gene / allele-specific silencing of mutant huntingtin. *Mol Ther* 19**,** 2178-2185.

Conroy, F., Miller, R., Alterman, J.F., Hassler, M.R., Echeverria, D., Godinho, B., Knox, E.G., Sapp, E., Sousa, J., Yamada, K., Mahmood, F., Boudi, A., Kegel-Gleason, K., Difiglia, M., Aronin, N., Khvorova, A., and Pfister, E.L. (2022). Chemical engineering of therapeutic siRNAs for allele-specific gene silencing in Huntington's disease models. *Nat Commun* 13**,** 5802.

Difiglia, M., Sapp, E., Chase, K., Schwarz, C., Meloni, A., Young, C., Martin, E., Vonsattel, J.P., Carraway, R., Reeves, S.A., and Et Al. (1995). Huntingtin is a cytoplasmic protein associated with vesicles in human and rat brain neurons. *Neuron* 14**,** 1075-1081.

Difiglia, M., Sena-Esteves, M., Chase, K., Sapp, E., Pfister, E., Sass, M., Yoder, J., Reeves, P., Pandey, R.K., Rajeev, K.G., Manoharan, M., Sah, D.W., Zamore, P.D., and Aronin, N. (2007). Therapeutic silencing of mutant huntingtin with siRNA attenuates striatal and cortical neuropathology and behavioral deficits. *Proc Natl Acad Sci U S A* 104**,** 17204-17209.

Dimovasili, C., Vitantonio, A.T., Conner, B., Vaughan, K.L., Mattison, J.A., and Rosene, D.L. (2024). White matter lipid alterations during aging in the rhesus monkey brain. *Geroscience*.

Dunah, A.W., Jeong, H., Griffin, A., Kim, Y.M., Standaert, D.G., Hersch, S.M., Mouradian, M.M., Young, A.B., Tanese, N., and Krainc, D. (2002). Sp1 and TAFII130 transcriptional activity disrupted in early Huntington's disease. *Science* 296**,** 2238-2243.

Fienko, S., Landles, C., Sathasivam, K., Mcateer, S.J., Milton, R.E., Osborne, G.F., Smith, E.J., Jones, S.T., Bondulich, M.K., Danby, E.C.E., Phillips, J., Taxy, B.A., Kordasiewicz, H.B., and Bates, G.P. (2022). Alternative processing of human HTT mRNA with implications for Huntington's disease therapeutics. *Brain* 145**,** 4409-4424.

Gao, G., Alvira, M.R., Somanathan, S., Lu, Y., Vandenberghe, L.H., Rux, J.J., Calcedo, R., Sanmiguel, J., Abbas, Z., and Wilson, J.M. (2003). Adeno-associated viruses undergo substantial evolution in primates during natural infections. *Proc Natl Acad Sci U S A* 100**,** 6081-6086.

Genetic Modifiers of Huntington's Disease Consortium. Electronic Address, G.H.M.H.E., and Genetic Modifiers of Huntington's Disease, C. (2019). CAG Repeat Not Polyglutamine Length Determines Timing of Huntington's Disease Onset. *Cell* 178**,** 887-900 e814.

Gu, Z. (2022). Complex heatmap visualization. *Imeta* 1**,** e43.

Hebb, A.L., Robertson, H.A., and Denovan-Wright, E.M. (2004). Striatal phosphodiesterase mRNA and protein levels are reduced in Huntington's disease transgenic mice prior to the onset of motor symptoms. *Neuroscience* 123**,** 967-981.

Hyeon, J.W., Kim, A.H., and Yano, H. (2021). Epigenetic regulation in Huntington's disease. *Neurochem Int* 148**,** 105074.

Iuliano, M., Seeley, C., Sapp, E., Jones, E.L., Martin, C., Li, X., Difiglia, M., and Kegel-Gleason, K.B. (2021). Disposition of Proteins and Lipids in Synaptic Membrane Compartments Is Altered in Q175/Q7 Huntington's Disease Mouse Striatum. *Front Synaptic Neurosci* 13**,** 618391.

Karpievitch, Y.V., Nikolic, S.B., Wilson, R., Sharman, J.E., and Edwards, L.M. (2014). Metabolomics data normalization with EigenMS. *PLoS One* 9**,** e116221.

Keeler, A.M., Sapp, E., Chase, K., Sottosanti, E., Danielson, E., Pfister, E., Stoica, L., Difiglia, M., Aronin, N., and Sena-Esteves, M. (2016). Cellular Analysis of Silencing the Huntington's Disease Gene Using AAV9 Mediated Delivery of Artificial Micro RNA into the Striatum of Q140/Q140 Mice. *J Huntingtons Dis* 5**,** 239-248.

Kegel, K.B., Meloni, A.R., Yi, Y., Kim, Y.J., Doyle, E., Cuiffo, B.G., Sapp, E., Wang, Y., Qin, Z.H., Chen, J.D., Nevins, J.R., Aronin, N., and Difiglia, M. (2002). Huntingtin is present in the nucleus, interacts with the transcriptional corepressor C-terminal binding protein, and represses transcription. *J Biol Chem* 277**,** 7466-7476.

Kegel, K.B., Sapp, E., Yoder, J., Cuiffo, B., Sobin, L., Kim, Y.J., Qin, Z.H., Hayden, M.R., Aronin, N., Scott, D.L., Isenberg, G., Goldmann, W.H., and Difiglia, M. (2005). Huntingtin associates with acidic phospholipids at the plasma membrane. *J Biol Chem* 280**,** 36464-36473.

Ko, J., Isas, J.M., Sabbaugh, A., Yoo, J.H., Pandey, N.K., Chongtham, A., Ladinsky, M., Wu, W.L., Rohweder, H., Weiss, A., Macdonald, D., Munoz-Sanjuan, I., Langen, R., Patterson, P.H., and Khoshnan, A. (2018). Identification of distinct conformations associated with monomers and fibril assemblies of mutant huntingtin. *Hum Mol Genet* 27**,** 2330-2343.

Koch, E.T., Cheng, J., Ramandi, D., Sepers, M.D., Hsu, A., Fong, T., Murphy, T.H., Yttri, E., and Raymond, L.A. (2024). Deep behavioural phenotyping of the Q175 Huntington disease mouse model: effects of age, sex, and weight. *BMC Biol* 22**,** 121.

Kordasiewicz, H.B., Stanek, L.M., Wancewicz, E.V., Mazur, C., Mcalonis, M.M., Pytel, K.A., Artates, J.W., Weiss, A., Cheng, S.H., Shihabuddin, L.S., Hung, G., Bennett, C.F., and Cleveland, D.W. (2012). Sustained therapeutic reversal of Huntington's disease by transient repression of huntingtin synthesis. *Neuron* 74**,** 1031-1044.

Landles, C., Sathasivam, K., Weiss, A., Woodman, B., Moffitt, H., Finkbeiner, S., Sun, B., Gafni, J., Ellerby, L.M., Trottier, Y., Richards, W.G., Osmand, A., Paganetti, P., and Bates, G.P. (2010). Proteolysis of mutant huntingtin produces an exon 1 fragment that accumulates as an aggregated protein in neuronal nuclei in Huntington disease. *J Biol Chem* 285**,** 8808-8823.

Langfelder, P., Cantle, J.P., Chatzopoulou, D., Wang, N., Gao, F., Al-Ramahi, I., Lu, X.H., Ramos, E.M., El-Zein, K., Zhao, Y., Deverasetty, S., Tebbe, A., Schaab, C., Lavery, D.J., Howland, D., Kwak, S., Botas, J., Aaronson, J.S., Rosinski, J., Coppola, G., Horvath, S., and Yang, X.W. (2016). Integrated genomics and proteomics define huntingtin CAG length-dependent networks in mice. *Nat Neurosci* 19**,** 623-633.

Lee, J.M., Huang, Y., Orth, M., Gillis, T., Siciliano, J., Hong, E., Mysore, J.S., Lucente, D., Wheeler, V.C., Seong, I.S., Mclean, Z.L., Mills, J.A., Mcallister, B., Lobanov, S.V., Massey, T.H., Ciosi, M., Landwehrmeyer, G.B., Paulsen, J.S., Dorsey, E.R., Shoulson, I., Sampaio, C., Monckton, D.G., Kwak, S., Holmans, P., Jones, L., Macdonald, M.E., Long, J.D., and Gusella, J.F. (2022). Genetic modifiers of Huntington disease differentially influence motor and cognitive domains. *Am J Hum Genet* 109**,** 885-899.

Lee, J.M., Zhang, J., Su, A.I., Walker, J.R., Wiltshire, T., Kang, K., Dragileva, E., Gillis, T., Lopez, E.T., Boily, M.J., Cyr, M., Kohane, I., Gusella, J.F., Macdonald, M.E., and Wheeler, V.C. (2010). A novel approach to investigate tissue-specific trinucleotide repeat instability. *BMC Syst Biol* 4**,** 29.

Luthi-Carter, R., Strand, A., Peters, N.L., Solano, S.M., Hollingsworth, Z.R., Menon, A.S., Frey, A.S., Spektor, B.S., Penney, E.B., Schilling, G., Ross, C.A., Borchelt, D.R., Tapscott, S.J., Young, A.B., Cha, J.H., and Olson, J.M. (2000). Decreased expression of striatal signaling genes in a mouse model of Huntington's disease. *Hum Mol Genet* 9**,** 1259-1271.

Marchionini, D.M., Liu, J.P., Ambesi-Impiombato, A., Kerker, K., Cirillo, K., Bansal, M., Mushlin, R., Brunner, D., Ramboz, S., Kwan, M., Kuhlbrodt, K., Tillack, K., Peters, F., Rauhala, L., Obenauer, J., Greene, J.R., Hartl, C., Khetarpal, V., Lager, B., Rosinski, J., Aaronson, J., Alam, M., Signer, E., Munoz-Sanjuan, I., Howland, D., and Zeitlin, S.O. (2022). Benefits of global mutant huntingtin lowering diminish over time in a Huntington's disease mouse model. *JCI Insight* 7.

Mathews, E.W., Coffey, S.R., Gärtner, A., Belgrad, J., Bragg, R.M., O'reilly, D., Cantle, J.P., Mchugh, C., Summers, A., Fentz, J., Schwagarus, T., Cornelius, A., Lingos, I., Burch, Z., Kovalenko, M., Andrew, M.A., Bennett, F.C., Kordasiewicz, H.B., Marchionini, D.M., Wilkinson, H., Vogt, T.F., Pinto, R.M., Khvorova, A., Howland, D., Wheeler, V.C., and Carroll, J.B. (2024). Suppression of Huntington's Disease Somatic Instability by Transcriptional Repression and Direct CAG Repeat Binding. *bioRxiv*.

Mathkar, P.P., Suresh, D., Dunn, J., Tom, C.M., and Mattis, V.B. (2019). Characterization of Neurodevelopmental Abnormalities in iPSC-Derived Striatal Cultures from Patients with Huntington's Disease. *J Huntingtons Dis* 8**,** 257-269.

Matyash, V., Liebisch, G., Kurzchalia, T.V., Shevchenko, A., and Schwudke, D. (2008). Lipid extraction by methyl-tert-butyl ether for high-throughput lipidomics. *J Lipid Res* 49**,** 1137-1146.

Menalled, L.B., Kudwa, A.E., Miller, S., Fitzpatrick, J., Watson-Johnson, J., Keating, N., Ruiz, M., Mushlin, R., Alosio, W., Mcconnell, K., Connor, D., Murphy, C., Oakeshott, S., Kwan, M., Beltran, J., Ghavami, A., Brunner, D., Park, L.C., Ramboz, S., and Howland, D. (2012). Comprehensive behavioral and molecular characterization of a new knock-in mouse model of Huntington's disease: zQ175. *PLoS One* 7**,** e49838.

Menalled, L.B., Sison, J.D., Dragatsis, I., Zeitlin, S., and Chesselet, M.F. (2003). Time course of early motor and neuropathological anomalies in a knock-in mouse model of Huntington's disease with 140 CAG repeats. *J Comp Neurol* 465**,** 11-26.

Peng, Q., Wu, B., Jiang, M., Jin, J., Hou, Z., Zheng, J., Zhang, J., and Duan, W. (2016). Characterization of Behavioral, Neuropathological, Brain Metabolic and Key Molecular Changes in zQ175 Knock-In Mouse Model of Huntington's Disease. *PLoS One* 11**,** e0148839.

Phillips, G.R., Saville, J.T., Hancock, S.E., Brown, S.H.J., Jenner, A.M., Mclean, C., Fuller, M., Newell, K.A., and Mitchell, T.W. (2022). The long and the short of Huntington's disease: how the sphingolipid profile is shifted in the caudate of advanced clinical cases. *Brain Commun* 4**,** fcab303.

Ross, C.A., and Tabrizi, S.J. (2011). Huntington's disease: from molecular pathogenesis to clinical treatment. *Lancet Neurol* 10**,** 83-98.

Sapp, E., Seeley, C., Iuliano, M., Weisman, E., Vodicka, P., Difiglia, M., and Kegel-Gleason, K.B. (2020). Protein changes in synaptosomes of Huntington's disease knock-in mice are dependent on age and brain region. *Neurobiol Dis* 141**,** 104950.

Sathasivam, K., Neueder, A., Gipson, T.A., Landles, C., Benjamin, A.C., Bondulich, M.K., Smith, D.L., Faull, R.L., Roos, R.A., Howland, D., Detloff, P.J., Housman, D.E., and Bates, G.P. (2013). Aberrant splicing of HTT generates the pathogenic exon 1 protein in Huntington disease. *Proc Natl Acad Sci U S A* 110**,** 2366-2370.

Shing, K., Sapp, E., Boudi, A., Liu, S., Seeley, C., Marchionini, D., Difiglia, M., and Kegel-Gleason, K.B. (2023). Early whole-body mutant huntingtin lowering averts changes in proteins and lipids important for synapse function and white matter maintenance in the LacQ140 mouse model. *Neurobiol Dis* 187**,** 106313.

Southwell, A.L., Kordasiewicz, H.B., Langbehn, D., Skotte, N.H., Parsons, M.P., Villanueva, E.B., Caron, N.S., Ostergaard, M.E., Anderson, L.M., Xie, Y., Cengio, L.D., Findlay-Black, H., Doty, C.N., Fitsimmons, B., Swayze, E.E., Seth, P.P., Raymond, L.A., Frank Bennett, C., and Hayden, M.R. (2018). Huntingtin suppression restores cognitive function in a mouse model of Huntington's disease. *Sci Transl Med* 10.

Southwell, A.L., Smith-Dijak, A., Kay, C., Sepers, M., Villanueva, E.B., Parsons, M.P., Xie, Y., Anderson, L., Felczak, B., Waltl, S., Ko, S., Cheung, D., Dal Cengio, L., Slama, R., Petoukhov, E., Raymond, L.A., and Hayden, M.R. (2016). An enhanced Q175 knock-in mouse model of Huntington disease with higher mutant huntingtin levels and accelerated disease phenotypes. *Hum Mol Genet* 25**,** 3654-3675.

Stanek, L.M., Yang, W., Angus, S., Sardi, P.S., Hayden, M.R., Hung, G.H., Bennett, C.F., Cheng, S.H., and Shihabuddin, L.S. (2013). Antisense oligonucleotide-mediated correction of transcriptional dysregulation is correlated with behavioral benefits in the YAC128 mouse model of Huntington's disease. *J Huntingtons Dis* 2**,** 217-228.

Steffan, J.S., Kazantsev, A., Spasic-Boskovic, O., Greenwald, M., Zhu, Y.Z., Gohler, H., Wanker, E.E., Bates, G.P., Housman, D.E., and Thompson, L.M. (2000). The Huntington's disease protein interacts with p53 and CREB-binding protein and represses transcription. *Proc Natl Acad Sci U S A* 97**,** 6763-6768.

Sun, Y., Tong, H., Yang, T., Liu, L., Li, X.J., and Li, S. (2022). Insights into White Matter Defect in Huntington's Disease. *Cells* 11.

Suopanki, J., Gotz, C., Lutsch, G., Schiller, J., Harjes, P., Herrmann, A., and Wanker, E.E. (2006). Interaction of huntingtin fragments with brain membranes--clues to early dysfunction in Huntington's disease. *J Neurochem* 96**,** 870-884.

Valencia, A., Sapp, E., Kimm, J.S., Mcclory, H., Ansong, K.A., Yohrling, G., Kwak, S., Kegel, K.B., Green, K.M., Shaffer, S.A., Aronin, N., and Difiglia, M. (2013). Striatal synaptosomes from Hdh140Q/140Q knock-in mice have altered protein levels, novel sites of methionine oxidation, and excess glutamate release after stimulation. *J Huntingtons Dis* 2**,** 459-475.

Vodicka, P., Lim, J., Williams, D.T., Kegel, K.B., Chase, K., Park, H., Marchionini, D., Wilkinson, S., Mead, T., Birch, H., Yates, D., Lyons, K., Dominguez, C., Beconi, M., Yue, Z., Aronin, N., and Difiglia, M. (2014). Assessment of chloroquine treatment for modulating autophagy flux in brain of WT and HD mice. *J Huntingtons Dis* 3**,** 159-174.

Weiss, A., Klein, C., Woodman, B., Sathasivam, K., Bibel, M., Regulier, E., Bates, G.P., and Paganetti, P. (2008). Sensitive biochemical aggregate detection reveals aggregation onset before symptom development in cellular and murine models of Huntington's disease. *J Neurochem* 104**,** 846-858.

Wheeler, V.C., White, J.K., Gutekunst, C.A., Vrbanac, V., Weaver, M., Li, X.J., Li, S.H., Yi, H., Vonsattel, J.P., Gusella, J.F., Hersch, S., Auerbach, W., Joyner, A.L., and Macdonald, M.E. (2000). Long glutamine tracts cause nuclear localization of a novel form of huntingtin in medium spiny striatal neurons in HdhQ92 and HdhQ111 knock-in mice. *Hum Mol Genet* 9**,** 503-513.

Zeitler, B., Froelich, S., Marlen, K., Shivak, D.A., Yu, Q., Li, D., Pearl, J.R., Miller, J.C., Zhang, L., Paschon, D.E., Hinkley, S.J., Ankoudinova, I., Lam, S., Guschin, D., Kopan, L., Cherone, J.M., Nguyen, H.B., Qiao, G., Ataei, Y., Mendel, M.C., Amora, R., Surosky, R., Laganiere, J., Vu, B.J., Narayanan, A., Sedaghat, Y., Tillack, K., Thiede, C., Gartner, A., Kwak, S., Bard, J., Mrzljak, L., Park, L., Heikkinen, T., Lehtimaki, K.K., Svedberg, M.M., Haggkvist, J., Tari, L., Toth, M., Varrone, A., Halldin, C., Kudwa, A.E., Ramboz, S., Day, M., Kondapalli, J., Surmeier, D.J., Urnov, F.D., Gregory, P.D., Rebar, E.J., Munoz-Sanjuan, I., and Zhang, H.S. (2019). Allele-selective transcriptional repression of mutant HTT for the treatment of Huntington's disease. *Nat Med* 25**,** 1131-1142.

Zhang, Y., Liu, Y., Sun, J., Zhang, W., Guo, Z., and Ma, Q. (2023). Arachidonic acid metabolism in health and disease. *MedComm (2020)* 4**,** e363.

Zuccato, C., Tartari, M., Crotti, A., Goffredo, D., Valenza, M., Conti, L., Cataudella, T., Leavitt, B.R., Hayden, M.R., Timmusk, T., Rigamonti, D., and Cattaneo, E. (2003). Huntingtin interacts with REST/NRSF to modulate the transcription of NRSE-controlled neuronal genes. *Nat Genet* 35**,** 76-83.